NASA
Technical
Paper
2555

January 1986

NASA-TP-2555 19860012919

Optical Elements Formed by Compressed Gases

Analysis and Potential Applications

Walton L. Howes

NASA

Optical Elements Formed by Compressed Gases

Analysis and Potential Applications

Walton L. Howes

Lewis Research Center
Cleveland, Ohio

Summary

Spherical, cylindrical, and conical shock waves are optically analogous to gas lenses. The geometrical optics of these shock configurations are analyzed as they pertain to flow visualization instruments, particularly the rainbow schlieren apparatus and single-pass interferometers. It is proposed that a lens or mirror formed by gas compressed between plastic sheets has potential as a fluid visualization test object, as the objective mirror in a very large space-based telescope, communication antenna, or energy collector; as the objective mirror in inexpensive commercial telescopes; and as a component in fluid visualization apparatuses.

Introduction

A gas lens is one in which the refracting medium consists of a gas rather than a rigid medium such as glass. If one surface of a flexible container of gas is reflecting, then a gas supported mirror is obtained. Gas lenses may occur as a consequence of natural phenomena such as shock waves or may be manufactured. In this report examples of gas lenses and gas-supported mirrors are discussed, and an elementary analysis of the optics is presented in order to illustrate characteristics of gaseous optical elements. The gas lenses and mirrors to be described result from pressurization of a lens-shaped volume of gas rather than as a consequence of a thermal boundary layer in a flowing heated gas (ref. 1). The construction of gas-supported mirrors has been studied intermittently at the NASA Langley Research Center since 1958, if not earlier.

Of the configurations discussed in this report, two result from natural phenomena, namely shock waves, and the others are devices which may potentially use gas lenses or mirrors advantageously.

The natural phenomena include the following:

(1) Spherical or cylindrical explosion waves

(2) Conical shock waves due to supersonic flow past a disturbing object.

Rainbow schlieren photographs of these phenomena can be evaluated by treating them as gas lenses.

The devices are as follows:

(1) A small gas lens to serve as a refracting object in a schlieren apparatus or as a phase object in an interferometer. A standard refracting object is useful as a test object for schlieren and interferometer apparatuses. Symmetric refracting objects which are weak refractors are not readily available. Gas lenses might be suitable for this purpose, especially since the refraction is then controllable by varying the gas pressure and temperature. This application was suggested by Josef Stricker, of the Technion-Israel Institute of Technology, Haifa, Israel.

(2) A very large gas-supported focussing mirror to serve as an optical objective in a very large, very high resolution, very lightweight, relatively inexpensive, space-based astronomical telescope or in a space-based, solar collector for power generation. Because of its lightweight, simplicity, and relatively low cost, a very large gas lens might serve as a reflecting optical objective for a high-resolution, space-based, astronomical telescope by making one lens surface reflecting. A similar mirror as a solar collector would have to satisfy less severe optical requirements.

(3) A lightweight, inexpensive, spherical mirror for use in large telescopes for personal use.

(4) A large, lightweight, inexpensive, easily manufactured, adjustable-focal-length mirror as a component in instruments for fluid visualization.

These ideas originated with the desire to extend the usefulness of the rainbow schlieren as a quantitative device to evaluate shockwave phenomena. It was immediately evident that the shock-wave configurations corresponded to lenses, so that standard light-ray-trace equations could be used to evaluate the shock waves.

Since the work on shock waves has progressed farthest, it is discussed first as it applies to the rainbow schlieren apparatus.

Rainbow Schlieren

The schlieren method for evaluating nonuniformities in fluids works by selective spatial filtering of light rays which are initially parallel to the optical axis but which are subsequently refracted by nonuniformities in the transparent medium under study. A diagram of the rainbow schlieren, which is completely described in references 2 and 3, is shown in figure 1. The principle of the rainbow schlieren is similar to that of the usual black-and-white schlieren except that the slit, light-source aperture is replaced by the smallest allowable pinhole
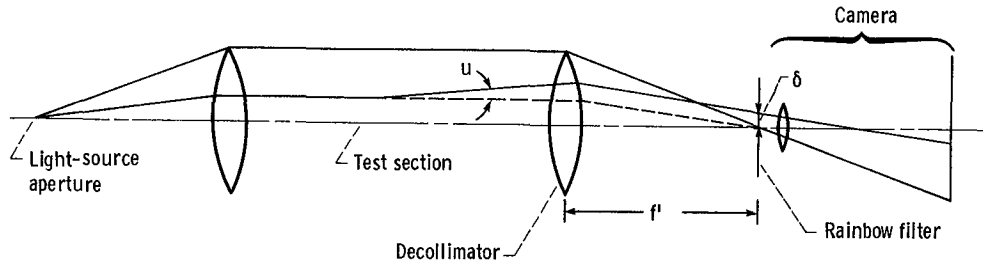
Figure 1.—Rainbow schlieren.

sufficient to permit a satisfactory photographic exposure of the test section. The usual knife-edge cutoff at the image of the light-source aperture is replaced by a radial rainbow filter consisting of a photographic color transparency. The filter possesses a clear center slightly larger than the image of the light source. The clear center is surrounded by a continuous radial rainbow with blue innermost and red outermost, encircled by an opaque outer surround.

Assume that the schlieren optics are ideal. If the refractive index in the test section is uniform, the image of the test section is white. However, wherever spatial nonuniformities of refractive index exist the traversing light is refracted and, hence, is deflected from the ideal image of the light-source aperture in the center of the filter. Consequently this light passes through a colored area of the filter, and so the corresponding region of the test section is imaged in color. Because the observed color can be associated with the magnitude of the light deflection at the filter, the color can be related to the magnitude of the nonuniformity in the test section if the nonuniformity possesses a simple geometry.

Suppose the object to be evaluated is a spherical, cylindrical, or conical shock wave. These fluid wave fronts and the consequent change in the values of gas properties behind the wave fronts correspond to gas lenses. Analysis of the optics of spherical, cylindrical, and conical gas lenses follows with particular attention to applications of the rainbow schlieren.

Spherical or Cylindrical Shock Wave

Shock waves may possess a wide variety of shapes (ref. 4). One common shock shape is spherical. Spherical shock waves arise from an explosion of a point or spherical source, or far from an extended explosive source, in a uniform stationary medium. A similar geometry (circular cross section) occurs in the case of an explosive line or cylindrical source. Explosion waves consist of an expanding discontinuity of fluid properties followed by a continuous gradient and eventual return, possibly via additional shocks, to ambient conditions.

As an approximation, the refraction of light due to the gradient behind a shock wave is assumed to be negligible compared with the refraction due to the shock wave

itself. Then the formulas for the optics of gas lenses are also valid for describing conditions immediately behind the shock.

By assuming that the shock wave is a step function, the problem of optical ray tracing is the same as that of lens design. With regard to the rainbow schlieren the procedure is the inverse of the lens design procedure. In lens design the media characteristics are given, and the ray traces are to be determined. In the rainbow-schlieren problem the ray deflections are determined experimentally, and the refractive index of the test medium is calculated therefrom.

In the rainbow schlieren, color in the image indicates that the light ray has been displaced by a distance δ at the rainbow filter (ref. 2 or 3). This displacement is related to the slope angle u (with respect to the optical axis of the schlieren system) of the ray trace emerging from the shock wave by the geometrical optics equation

$$u = \tan^{-1}\left(\frac{\delta}{f'}\right) \approx \left(\frac{\delta}{f'}\right) \tag{1}$$

where f' is the focal length of the decollimator (fig. 1), and $|u| < < \pi/2$ for a gas lens. (All quantities are defined in appendix A.) Because $|\delta| \propto f'$ the magnitude of δ in a schlieren apparatus can be increased by increasing f'. Equation (1) is independent of the cause of refraction in the test section. The remaining problem, which is analyzed in appendix B, is to relate u to the refractive index difference $n_2 - n_1$ across the shock wave.

Assume that $n_2 - n_1 < < 1$ across a shock wave. The refractive index n of a nonionized gas is related to its density ρ by the Gladstone-Dale equation (e.g., ref. 5):

$$n - 1 = k\rho \tag{2}$$

where $0.225 \times 10^{-3} < k < 0.230 \times 10^{-3}$ m³kg^{-1} for 700 $> \lambda > 400$ nm with λ the optical wavelength. For Mach numbers M ≤ 5, $\rho_2/\rho_1 \leq 5$, where the subscripts 1 and 2, respectively, refer to the medium ahead of and behind the shock wave. Hence, for example, using the preceding values gives $n_2 - n_1 = 1.17 \times 10^{-3} < < 1$ if $\lambda = 546.1$ nm (mercury green line). Many other fluid dynamic quantities can be calculated from ρ_2/ρ_1 (ref. 6).

Approximate solutions for $(n_2 - n_1)/n_2$ as a function of quantities measurable by using a rainbow-schlieren apparatus are derived in appendix B. The significant formulas are presented in the following paragraphs.

Thick lens paraxial solution.—At any refracting surface the incident light ray, surface normal, and refracted ray all lie in the same plane according to Snell's law of refraction. The center of the spherical shock wave also lies in this plane. For a circular cylinder of finite length the geometry is analogous if the incident light direction is normal or parallel to the axis of the cylinder (fig. 2). Consequently, the spherical or cylindrical shock wave acts like a thick, spherical gas lens. The paraxial (near the optical axis of the lens) equation for a lens having a thickness d is (ref. 7, p. 58)

$$\frac{1}{F'} = (n_2 - n_1)\left(\frac{1}{r_1} - \frac{1}{r_2} + \frac{n_2 - n_1}{n_2}\frac{d}{r_1 r_2}\right) \tag{3}$$

where F' is the focal length, and for a circular section

$$r_1 = -r_2 \equiv r$$

are the consecutive shock surface radii encountered by each light ray. (The notation and sign conventions are the same as in ref. 8 and fig. 3.) For a sphere, or cylinder (across its axis), the lens thickness $d > 0$ measured along the optical axis is given by $d = 2r$. As shown in appendix B, following appropriate substitutions, equation (3) reduces to

$$\epsilon \equiv \frac{n_2 - n_1}{n_2} = \frac{\delta}{2f'}\frac{r}{y_1} \tag{4}$$

if $u < < y_1/(d - 2r)$, where y_1 is the ordinate value of a ray trace as it first encounters the shock wave. The same result is obtained if it is assumed that $\epsilon < < 2r/d$, so that, for example, equation (4) is valid for $d/r < < 2 \times 10^3$ if $\epsilon \approx 10^{-3}$. Equation (4) expresses the relative refractive index difference ϵ across the shock discontinuity as a function of the deflection δ measurable with the rainbow schlieren.

In practice $d/r < < 2/\epsilon$, so that equation (4), which was derived for a spherical lens, is also valid for a thick gas lens bounded by spherical surfaces (appendix B). The shock wave radiated from a cylindrical source of finite length with the light path parallel to the cylinder axis (fig. 2) determines a lens of this type. Near the cylinder the shock wave is cylindrical around the cylindrical surface, a circular toroidal section near the cylinder edges, and plane near the cylinder ends (fig. 2). Far from the cylinder in comparison with its diameter the wave around the ends of the cylinder becomes hemispherical. Thus, if the incident light path is parallel to the cylinder axis, $d/r \geq 2$, and equation (4) is valid.

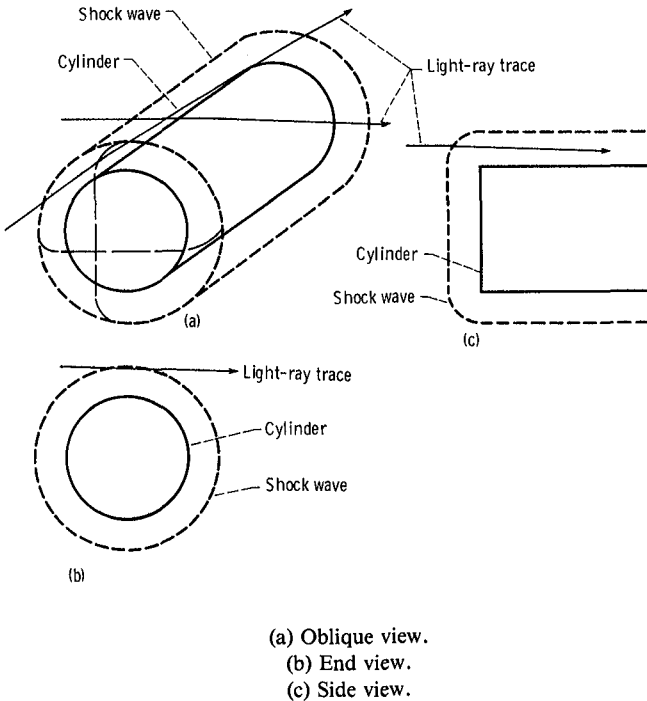(a) Oblique view.
(b) End view.
(c) Side view.

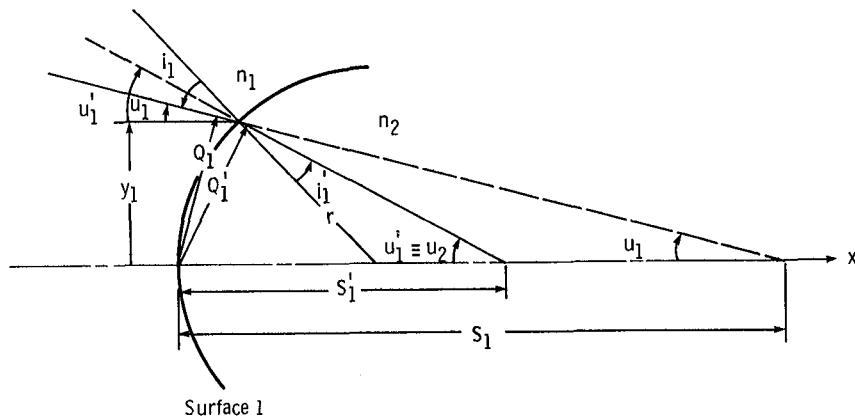Figure 2.—Shock shape and light paths near cylinder.

Figure 3.—Ray-trace convention. (All positive diagram.)

Although, with respect to the rainbow schlieren, equation (4) is not of practical use because it applies only near the optical axis and not, as desired, near tangency to the shock wave, equation (4) does provide a basis for the expected form of an axial equation for nonparaxial rays.

In order to properly evaluate ϵ, it is important that the test section image be undistorted. Assume that the schlieren optical system is ideal, hence distortion free. There nevertheless remains the important possibility of distortion of imagery of refractive index nonuniformities in the test section caused by the refraction they produce. (This distortion is not the usual optical distortion associated with imagery at large extra-axial angles, but rather is associated with all rays, axial and extra-axial, which traverse the refracting test medium.) This distortion is minimized by proper selection of the test-section object plane to be imaged. The distortion vanishes if the selected object plane coincides with the intersection of the forward and backward extensions of each ray trace, respectively, before and after traversing the test section. Thus, for vanishing distortion the selected object plane must coincide with the second (final) principal plane of the gas lens. The distance ξ_2 of the second principal plane from the second (final) shock surface encountered by the light is given by (ref. 7, p. 59)

$$\xi_2 = \frac{d\,r_2}{n_2(r_1 - r_2) - (n_2 - n_1)d}$$

$$= -\frac{d}{2} = -r$$

because $\epsilon \ll 1$. Thus, ξ_2 corresponds to the midspan plane of the test section which is also the fluid dynamic symmetry plane. Focusing on the midspan plane eliminates the distortion of nonuniformities for paraxial rays.

Axial ray solution from symmetry.—The axial ray solution for ϵ in a spherical gas lens $(d = 2r)$ is easily obtained by using Snell's law,

$$\frac{n_1}{n_2} = \frac{\sin i_1'}{\sin i_1} \tag{5}$$

where i_1 and i_1' are, respectively, the angles of incidence and refraction of a light ray at first encounter with the shock wave. The initial ray slope $u_1 = 0$ if the incident rays are parallel to the optical axis. It follows from the symmetry of the ray trace through the lens (fig. 4) that, as shown in appendix B,

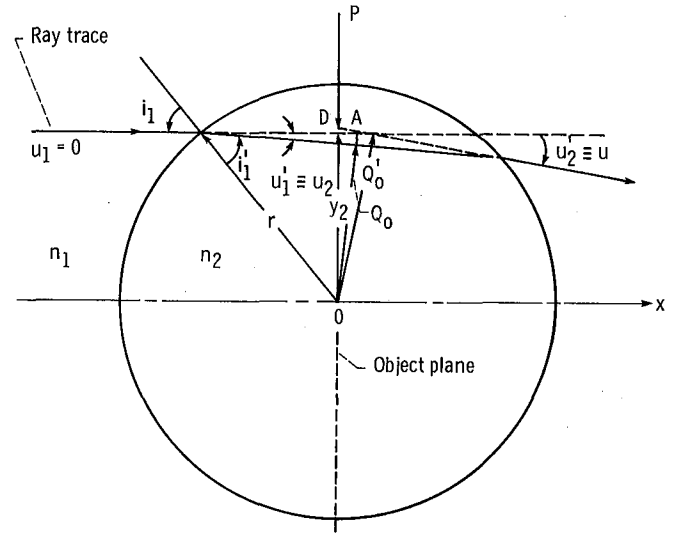$$\epsilon = \frac{\delta}{2f'} \frac{r}{y_1} \left[1 - \left(\frac{y_1}{r}\right)^2\right]^{1/2} \tag{6}$$

Figure 4.—Symmetry of ray trace through spherical or cylindrical shock wave.

for $|y_1/r| < 1$, where ϵ is expressed in terms of measurable quantities, f' from the apparatus, δ from the radius of the hue in the filter which matches that in the image of the test section, and r and y_1 from a color transparency of the image. Note that, since the quantities measured from the transparency occur in the form of dimensionless ratios in equation (6), the image magnification is not involved in calculating ϵ.

Except for the square-root term, equation (6) is identical to the paraxial equation (4).

According to equation (6) and all subsequent variations thereof, ϵ is indeterminate for $y_1/r = 0$ because there is no refraction for normal incidence at the shock (Snell's law), and, hence, $\delta = 0$. The rainbow-schlieren effect is only observed where $|i_1| \neq 0$. The refraction and, therefore, the deflection δ is maximized if $|i_1| \to \pi/2$, that is, immediately behind the image of the shock. This is where the image can be expected to be most colorful.

From figure 4 the optical distortion D at the object plane $\overline{OP}$, which contains the fluid symmetry axis, is given, as shown in appendix B, by

$$\frac{D}{y_1} = \tan u_1' \tan u_2'$$

$$= \frac{1}{2}\left(\frac{\delta}{f'}\right)^2 \approx 0 \tag{7}$$

for $|y_1/r| < 1$ because $|\delta/f'| \ll 1$. In practice the distortion is negligible if it does not exceed the accuracy of reading the color transparency.

As in the paraxial case, there is negligible distortion in the transformation from object to image in the presence of refraction by a spherical gas lens if the object plane contains the fluid symmetry point, or axis.

4

Axial ray trace solution.—The most general method of geometrical optics is ray tracing (ref. 8), which in the present instance can also be used to obtain explicit solutions for $\epsilon(u)$ for both paraxial and marginal rays.

For a spherical shock wave the ray-trace solution serves as a confirmation of the previous solution (eq. (6)) derived from symmetry considerations. For more complex wave shapes the ray-trace method may be the only method available for evaluating $\epsilon(u)$.

It is shown in appendix B that the method of ray tracing leads to the same results as before, namely,

$$\epsilon = \frac{\delta}{2f'} \frac{r}{y_1} \tag{4}$$

for paraxial rays, and

$$\epsilon = \frac{\delta}{2f'} \frac{r}{y_1} \left[1 - \left(\frac{y_1}{r} \right)^2 \right]^{1/2} \tag{6}$$

for nonparaxial rays, as it should. Also, as before

$$\frac{D}{y_1} = \frac{1}{2} \left(\frac{\delta}{f'} \right)^2 \tag{7}$$

Conical Shock Wave

A conical shock wave is produced by linear, uniform, supersonic relative motion between a body and the surrounding uniform medium. The body may be a point, may be axially symmetric with a pointed nose, or may be any body if the shock wave is far from the body in comparison with its largest dimension. Cross sections of the shock cone perpendicular to the ambient flow are assumed to be circular. According to Snell's law, at each shock surface, the plane of refraction includes the surface normal, which is not in the plane of the circular cross section, and the incident and refracted ray traces. An approximate solution for u must be found from ray-trace formulas since simpler approaches are not obvious. The problem is one of tracing axial rays through a conical gas lens, where the cone axis is perpendicular to the optical axis.

With the origin of coordinates at the vertex of the cone, as shown in figure 5(a), the formula for a cone is

$$X^2 + Y^2 = Z^2 \tan^2 \theta$$

where the Z-axis coincides with the cone axis, and θ is the cone angle. The X-axis is parallel to, and the Y-axis is perpendicular to, the initially incident light rays. For the optical problem it is more convenient to relocate the origin of the x-coordinate in an x,y,z-coordinate system at the point of incidence of the X-axis with the shock wave, so that

$$X = x - r$$

$$Y = y$$

$$Z = z$$

where r is the radius of the cone. Then, the equation of the cone becomes

$$x^2 - 2rx + r^2 + y^2 - z^2 \tan^2 \theta = 0$$

A given ray trace intersects the shock wave initially at $(x,y,z) = (x_1,y_1,z_1)$.
In terms of these coordinates it is shown in appendix C that

$$\epsilon = \frac{\delta \cot \theta}{2f'} \left[\frac{1 - (y_1/r_1)^2}{1 + (y_1/r_1)^2 \cot^2 \theta} \right]^{1/2} \tag{8}$$

for $0 \le \theta < \pi/2$ and $|y_1/r_1| < 1$, where r_1 is the radius of the cross section of the cone perpendicular to $z = z_1$. Equation (8) expresses the refractive index difference across a conical shock wave as a function of easily measurable quantities. For $\theta = 0$, equation (8) reduces to equation (6), which applies for a spherical shock wave. For $\theta = \pi/2$, $\epsilon = 0$.

If the camera is focused on the Y,Z-coordinate plane, the distortion D is given by the displacement in the plane $X = 0$ of the backward extension of the ray trace emerging at x_2, y_2, z_2 relative to its forward extension from x_1, y_1, z_1. Thus

$$D = \left[(Y_0 - y_1)^2 + (Z_0 - z_1)^2 \right]^{1/2}$$

where (Y_0, Z_0) are the coordinates of the backward extension at the object plane. Since

$$D = Y_0 - y_1 = \frac{y_1}{2} \left(\frac{\delta}{f'} \right)^2$$

for a sphere is negligible, for the cone, D must be of the same order of magnitude and, hence, must generally be negligible in this case also.

Gas Lens

It is often desirable to have a simple transparent object to test new versions of schlieren, interferometric, or other
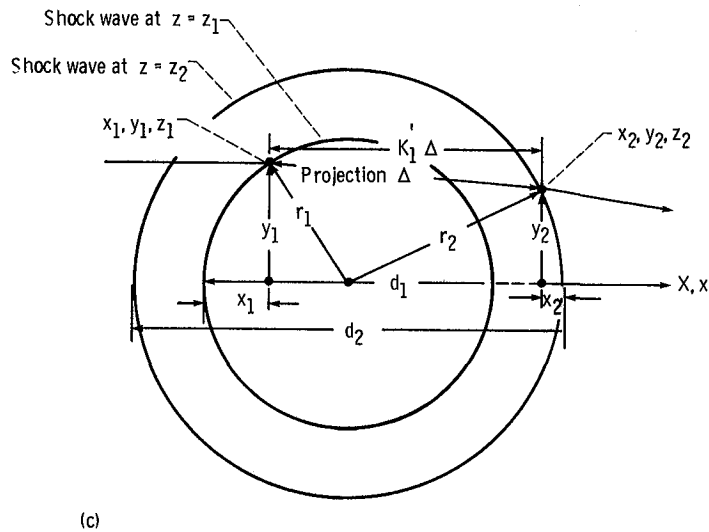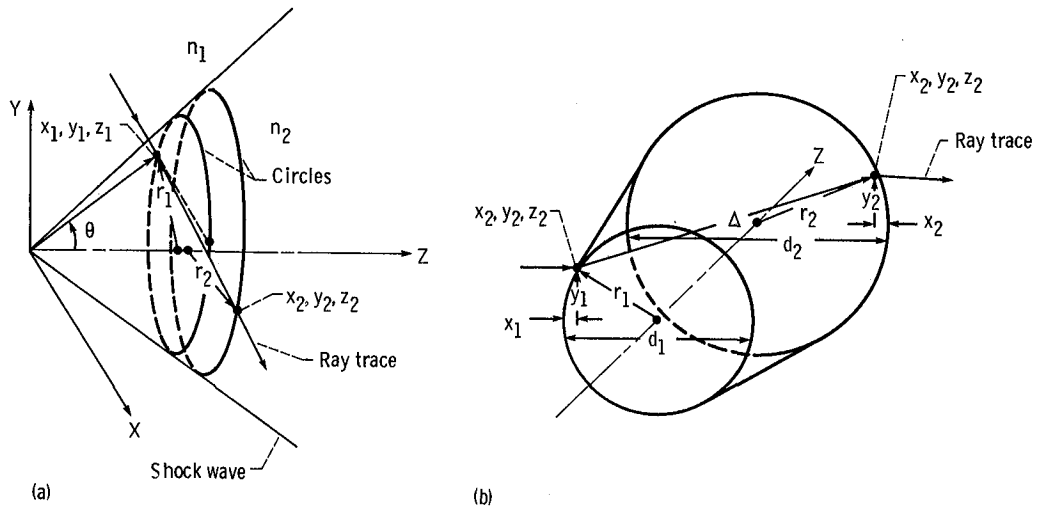
(a) Ray trace.
(b) Geometry for transfer formulas.
(c) Projection in plane Z = constant.

Figure 5.—Conical shock wave.

optical instruments used for visualizing or evaluating transparent media. For quantitative purposes the test object should provide a simple optical geometry. Free-convection flows over planes or cylinders and axially symmetric flames have been used. However, real flows are usually time dependent, so without simultaneous observations it is especially difficult to compare different instruments by using flows. Glass lenses, unless nearly planar, usually produce too much refraction to be useful. A nonlinear crystal has been used, but this is expensive and introduces the danger of large electric potentials (ref. 9).

Many advantages are inherent in gas lenses as test objects. A gas lens provides a simple geometric test object which, although time independent, can be readily adjusted to produce different amounts of refraction by adjusting the gas pressure or temperature within the lens. Gas lenses are simple, inexpensive, easily made, and scalable to any size desired.

A gas lens may consist simply of a transparent, spherical balloon. An advantageous alternative involves enclosing the ends of a metal cylinder with sheets of transparent plastic mounted to seal the cylinder. Gas injected through a valve in the cylinder wall deflects the plastic essentially into segments of spherical surfaces.

It follows from equation (3) that the focal length of a gas lens with radii $r_1 = -r_2 = r$ is given by

$$F' \approx \frac{r}{2\epsilon}$$

The f-number of the lens is given by

$$\text{f-number} = \frac{F'}{2r} = \frac{1}{4\epsilon}$$

Because $\epsilon = O(10^{-3})$, f-number $= O(10^2)$, where O refers to the order of magnitude. Therefore, although a gas lens may not have much value as a normal lens, it, nevertheless, may be useful as a test object.

When the rainbow schlieren and equation (6) are used, the refractive index difference ϵ for a gas lens can be evaluated if r is known.

The corresponding optical analysis for a gas lens and Mach-Zehnder interferometer is derived in appendix C, by using figure 6, where it is shown that the fringe shift S is given by

$$\frac{S}{2r[1-(y_1/r)^2]^{1/2}} = \frac{\epsilon}{\lambda} = \text{constant} \qquad (10)$$

Let $S = S(y_m)$ at the lens margin, $y_1 = y_m$ and let $S = S(0)$ on the optical axis, $y_1 = 0$. Successively introducing these pairs of values in equation (10) and taking the difference of the two equations give

$$\epsilon = \frac{(\Delta S)\lambda}{2r\left\{1-\left[1-\left(\dfrac{y_m}{r}\right)^2\right]^{1/2}\right\}} \qquad (11)$$

where $\Delta S = S(0) - S(y_m)$ is simply the number of fringes between the margin and center of the lens. This equation can be used to determine ϵ if r is known. For a sphere, $y_m = r$, so that
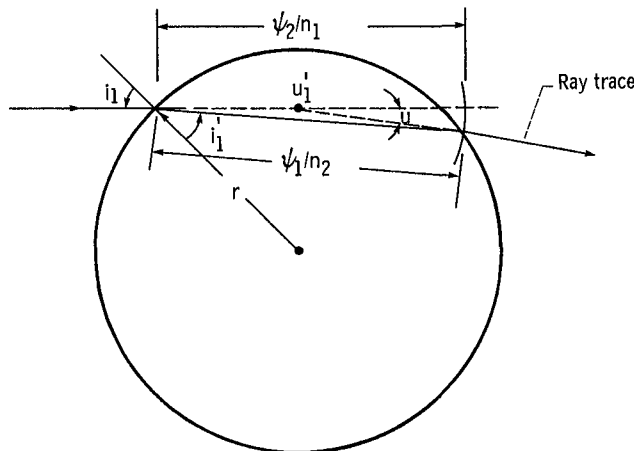
$$\epsilon = \frac{(\Delta S)\lambda}{2r}$$

Figure 6.—Ray traces through spherical lens for determining fringe shifts.

Note that equations (9) and (11) can be combined to yield the lens focal length

$$F' = \frac{r^2}{(\Delta S)\lambda}\left\{1-\left[1-\left(\frac{y_m}{r}\right)^2\right]\right\}$$

from interferometric measurements when ϵ is unknown.

In a preliminary test, a 2.54-cm-diameter gas lens was assembled as a test object. The lens surfaces were made of 0.02-mm-thick Mylar membranes spread across, and sealed by, aluminum rings. These membranes supported more than 5 atm of air pressure within the lens at the bursting point. At this pressure and atmospheric temperature, $\epsilon = O(10^{-3})$. Moreover, at this pressure the deflection of the originally flat Mylar was approximately equal to the radius of the containment ring as a result of stretching. The light perturbation caused by the lens was simultaneously observed with a Mach-Zehnder interferometer and a rainbow schlieren and found to be within the acceptable range of these instruments. No recordings or quantitative measurements were made. However, from visual observations it was evident that the lens surfaces were ellipsoidal rather than spherical, a consequence of the orthotropism of Mylar (ref. 10). These observations indicated that both instruments could be used to study nonisotropic stretching of the transparent lens surface or nonuniformity of its mounting around the periphery.

Gas-Supported Mirror

Although a gas-supported lens may have limited usefulness (ref. 11), a gas-supported mirror might have many uses (refs. 12 to 16). In principle a gas-supported focussing mirror might be used in any application where a metallic mirror on a glass substrate would ordinarily be used. Certain advantages and limitations of the gas mirror govern its potential uses and may allow applications where glass mirrors are impractical.

Some potential advantages of a gas-supported mirror are

(1) Simplicity
(2) Low cost
(3) Lightweight
(4) Ease of construction
(5) Adjustable focus
(6) Adjustable surface curvature
(7) Ease of achieving low f-number
(8) Reflecting surface automatically protected from dust

Among potential disadvantages are

(1) Reduced surface quality
(2) Increased light scattering

(3) Thermal sensitivity
(4) Deformation by acceleration
(5) Damage sensitivity
(6) Hysteresis
(7) Discoloration of surface
(8) Response to noise and vibration
(9) Deflection by gravity

The construction of a gas-supported mirror may be similar to that of a gas lens, except that in the mirror one surface is metallically coated for reflectance. If the coating is on the outside surface, the mirror is convex; whereas if the coating is on the inside surface, the mirror is concave. In the case of the concave mirror, which is of greatest interest, the incident light must traverse the transparent surface and internal gas twice. However, except when considering aberrations, the lens effect is insignificant because the gas pressure necessary to support the mirror is only slightly greater than ambient pressure. The deviation of the mirror from sphericity depends on the material, its thickness, the mounting technique, and whether or not the material is stretched. Thus, for best imagery local deformations of the surface from its natural shape are probably necessary.

The potential uses of a gas-supported mirror are dictated by the aforementioned advantages and disadvantages. Thus, a gas-supported mirror may be considered as a telescope objective in telescopes considerably larger than any yet conceived or as an antenna for a microwave receiver or transmitter (ref. 17). It may also be considered as a radiant flux-gathering antenna where imaging quality is not an important consideration (ref. 18). Because of its low cost a gas-supported mirror might be used as a large, low f-number objective in a personal telescope. In fluid visualization experiments (ref. 3) large focussing mirrors are frequently needed for a limited time in testing facilities with various dimensions. Because of their low cost, ease and speed of construction, and adjustability, gas-supported mirrors may be useful in these applications. Many other applications are possible.

The lowest wavelength for which a gas-supported mirror is usable is determined by the accuracy to which the desired surface shape can be maintained, the deflecting surface roughness, and probably the size of the scatterers within the transparent plastic lens surface.

Very Large Astronomical Telescope

The principal, potential optical advantages of a gas-supported mirror in this application are angular resolution and energy-gathering power. The angular resolution is given by $\theta = 1.22 \lambda/\mathfrak{D}$, where $\mathfrak{D}$ is the diameter of the entrance pupil. For example, a 300-m-diameter gas-supported telescope objective would have a theoretical resolving power more than 40 times that of the largest existing single-mirror telescope

objective. The energy-gathering power is proportional to $\mathfrak{D}^2$; hence it would be 1600 times that of the largest existing mirror. The greatest advantage of the gas mirror would be achieved as part of a space-based telescope, where most of the cited advantages would be overwhelming relative to the alternatives. However, most of the cited disadvantages would also be important and must be overcome.

In this potential application the gas supported plastic mirror is the central surface between two other plastic membranes, one of which is transparent. These membranes and the mirror are sealed together around their periphery by a metal, or inflated plastic, toroidal tube. The spaces between the membranes are inflated with a transparent, chemically inert gas to form two chambers. The gas in the front chamber supports the mirror by establishing a weak gas lens with the mirror as one surface. The space between the back membrane and the mirror is inflated to a lesser pressure than the front chamber. The back chamber might be subdivided into separate annuli which would be inflated independently to different pressures. The back surface of the mirror and the chamber separators are made from concentric annular membranes so that the mirror is of uniform thickness. The mirror is thicker than the surrounding membranes. The receiver is supported at the mirror focus by three metal, or inflated plastic, pylons extending from the toroidal rim of the mirror to the focus.

To support the entire system the internal gas pressure need be only slightly greater than ambient pressure. A valving system interconnects the various chambers so that pressure differentials may be controlled throughout the system.

The surface quality, light scattering characteristics, and discoloration of the plastic material may be the most serious limitations on the success of this telescope. Surface quality might be improved by surface coatings. Material selection would determine the scattering and discoloration characteristics.

Heating, especially differential heating, could be minimized by keeping the telescope out of the shadows of the Earth and Moon, slowly rotating the mirror about its optical axis, and coating the back side of the mirror, generally the sun side, to minimize heating. The compartmentalization of the back of the mirror would allow control over the shape of the mirror surface by means of differential gas pressure. The sensitivity of the mirror surface shape to gas pressure differentials could be optimized by making the mirror thickness different from that of the transparent membranes enclosing the mirror. Some telescopes use an aberration corrector plate in front of the mirror (ref. 19). It might be possible to achieve this effect by varying the thickness of the transmitting surface of the lens as a function of its radius. The gas-supported-mirror telescope should be relatively insensitive to particle damage because the gas pressure

differentials would be low. Thus, it should not be difficult to retain pressure to compensate for leaks. Hysteresis should not be a problem if the mirror is not stretched. Stretching can be minimized by mounting the membranes nonrigidly at the periphery. Acceleration, gravity, noise, and vibration should not be problems.

Preliminary tests using Mylar plastic indicate that light scattering by the plastic may significantly degrade optical performance at visible wavelengths.

Because the reflective coating is metallic, the mirror as a reflector should be effective from the ultraviolet well into the microwave region of the electromagnetic spectrum. The deleterious effects of the mirror surface would be less at the longer wavelengths.

Very Large Solar Energy Collector

Although the possibility exists that the image quality would not be satisfactory for a telescope, a very large gas-supported mirror might still be acceptable as a space-based solar collector. In a solar energy collector, image quality is not significant. All the potential advantages are retained, whereas the potential disadvantages are much less severe in the solar collector than they are in the telescope.

Personal Telescope

The principle advantage in this application is probably cost, since the mirror is the most expensive single item in telescopes. Thus, large, low f-number, lightweight, commercial telescopes might be manufactured at a fraction of the cost of their glass counterparts. All the cited advantages pertain, but all listed disadvantages other than light scattering and thermal sensitivity are likely to be insignificant.

Fluid Visualization (ref. 3)

All cited advantages apply in this application. Adjustable focus and surface curvature may be especially important in instrument applications because they allow one mirror to be used in a variety of situations involving different optical requirements. Most of the disadvantages are likely to be insignificant, although thermal sensitivity may be important in fluctuating thermal environments, and noise and vibration might be a serious problem in very noisy environments.

The gas lens reported in the section Gas Lens was easily converted into a concave, gas-supported mirror by replacing one surface of the lens with a plastic sheet with a highly reflecting coating. Preliminary observations of the image of a point source at infinity indicated good image quality. However, significant scattered light was observed around the point image.

The preceding applications illustrate only a few possibilities. Undoubtedly there exist many other potential applications of gas lenses and gas-supported mirrors.

Conclusion

The geometrical optics of spherical, cylindrical, and conical shock waves have been analyzed as they relate to flow visualization instruments, especially the schlieren apparatus and interferometer. The shock configurations are analogous to gas lenses. From these results and a preliminary test of a small gas lens it is proposed that a gas lens might serve as a useful test object for evaluating flow visualization devices. From preliminary tests of a gas-supported mirror it is proposed that a gas-supported mirror might be a suitable objective for a space-based telescope far larger than any yet conceived. In addition, gas-supported mirrors might be satisfactory as very large solar collectors or microwave antennas and in inexpensive personal telescopes.

Appendix A
Symbols

A $\pm a(1-a'^2)^{1/2} \mp a'(1-a^2)^{1/2}$

a y/r, for spherical or cylindrical lens

a' $(n_2/n_1)a$, for spherical or cylindrical lens

a_1 y_1/r_1, for conical lens

a_2 y_2/r_2, for conical lens

B $\mp b(1-b'^2)^{1/2} \pm b'(1-b^2)^{1/2}$

b $Q_2/r_2 - A$

b' $(n_2/n_1)b$

D distortion

$\mathcal{D}$ diameter of entrance pupil

d thickness of spherical lens; thickness of conical lens in plane indicated by subscript (fig. 5(b))

F' focal length of gas lens

F_m focal length of mirror

$\mathcal{F}$ $\dfrac{K_1'[x_1 - \frac{1}{2}(d_1+d_2)] + L_1'y_1 - M_1'z_1 \tan^2\theta}{K_1'^2 + L_1'^2 - M_1'^2 \tan^2\theta}$

f' focal length of schlieren decollimator

$\mathcal{G}$ $\dfrac{[x_1 - \frac{1}{2}(d_1+d_2)]^2 + y_1^2 - z_1^2 \tan^2\theta}{K_1'^2 + L_1'^2 - M_1'^2 \tan^2\theta}$

g $(x-r)^2 + y^2 - z^2 \tan^2\theta = 0$, for cone

h $\dfrac{(1 + a_1 a_2 \cot^2\theta) \tan^2\theta}{[(1-a_1^2)(1-a_2^2)]^{1/2}}$

i angle of incidence

i' angle of refraction

J_1 $n_2 \cos i_1' - n_1 \cos i_1$

J_2 $n_1 \cos i_2' - n_2 \cos i_2$

K,L,M direction cosines of ray trace

k Gladstone-Dale constant

k,l,m direction cosines of normal to shock wave surface at point of incidence of ray trace

M Mach number

$\mathbf{N}$ unit normal vector to shock wave surface

n refractive index

O order of magnitude

Q distance normal to ray trace from vertex formed by optical axis and shock wave surface

Q_o distance normal to ray trace from center of spherical or cylindrical lens

$\hat{\mathbf{R}}$ unit vector along ray trace

r radius

S interference fringe shift

ΔS $S(y=0) - S(y_m)$

s distance from ray-trace shock-wave intersection to ray-trace optical-axis intersection measured along optical axis

u slope angle of ray trace with respect to optical axis

X,Y,Z rectangular coordinates of cone surface (Z-axis is cone axis)

x,y,z rectangular coordinates of ray trace (x-axis is optical axis)

y_m ordinate value of ray trace at lens margin

α if $\alpha_1 \approx \alpha_2$

α_1 $1 - a_1^2$

α_2 $1 - a_2^2$

Δ physical length of ray trace within lens

δ displacement of ray-trace normal to optical axis at image of light source in schlieren apparatus

ϵ $(n_2 - n_1)/n_2$

θ cone semiangle

λ wavelength

ξ distance of principal plane from vertex formed by lens surface and optical axis

ρ gas density

φ $\pi/2 \pm$ angle of incidence

ψ optical path length

Subscripts:

0   at object plane

1   outside, left side, or first surface contact

2   inside, right side, or second surface contact

Superscripts:

$\hat{\ }$ unit vector

$'$ to right of refracting surface

Appendix B

Optical Formulas for Thick Gas Lenses

Spherical Lens

Thick lens paraxial solution.—In terms of light-ray traces in the object and image spaces, the focal length F' of a lens is given by

$$F' = \frac{y_1}{\sin u} \approx \frac{y_1}{u}$$

for paraxial rays, where $|u| << \pi/2$, and y_1 is the initial height of an axial ray measured perpendicular to the optical (x) axis. When this formula is combined with the thick lens equation,

$$\frac{1}{F'} = (n_2 - n_1)\left(\frac{1}{r_1} - \frac{1}{r_2} + \frac{n_2 - n_1}{n_2}\frac{d}{r_1 r_2}\right) \tag{3}$$

and F' is eliminated, the result is

$$\frac{u}{y_1} = n_2 \epsilon \left(\frac{2}{r} - \epsilon \frac{d}{r^2}\right)$$

where

$$\epsilon \equiv \frac{n_2 - n_1}{n_2}$$

and it is assumed that $r_1 = -r_2 = r$, that is, the surface radii are equal in magnitude. For $\epsilon << 1$, $n_2 = n_1/(1 - \epsilon) \approx n_1(1 + \epsilon)$, and the preceding result leads to the quadratic equation for ϵ,

$$\left(\frac{d - 2r}{r^2}\right)\epsilon^2 - \frac{2}{r}\epsilon + \frac{u}{n_1 y_1} = 0$$

The solution of this quadratic equation is

$$\epsilon = \frac{r}{(d - 2r)}\left\{1 \pm \left[1 - (d - 2r)\frac{u}{n_1 y_1}\right]^{1/2}\right\}$$

$$\approx \frac{u}{2n_1}\frac{r}{y_1}$$

if

$$u << \frac{y_1}{d - 2r}$$

Combining equation (1), namely,

$$u \approx \frac{\delta}{f'} \tag{1}$$

with the approximate solution of the quadratic equation gives the desired representation for ϵ,

$$\epsilon = \frac{\delta}{2f'}\frac{r}{y_1} \tag{4}$$

Under the preceding assumptions, it follows from equation (3) that the focal length of a gas lens is approximated by

$$F' = \frac{r}{2\epsilon} \tag{B1}$$

if $\epsilon << 2r/d$. This is closely related to

$$F'_m = \frac{r_m}{2}$$

for the focal length F'_m of a spherical mirror with a radius r_m. Thus, if $r = r_m$, $F' = F'_m/\epsilon$, so that the focal length of the spherical gas lines formed by a shock wave is $O(10^3)$ times that of a spherical mirror with the same radius. (The symbol O stands for the order of magnitude.)

Eliminating ϵ from equations (4) and (B1) relates focal lengths F' and f' of the gas lens and schlieren decollimator; that is,

$$\frac{F'}{f'} = \frac{y_1}{\delta}$$

Generally $F' >> f'$, so that $|y_1| >> |\delta|$.

Axial ray solution from symmetry.—In figure 4,

$$i'_1 = i_1 + u_1 - u'_1$$

where u_1 and u'_1 are the ray slope angles before and after refraction, respectively. Since

$$u_1 = 0$$

because the incident rays are parallel to the optical axis, Snell's law (eq. (5)) becomes

$$\frac{n_1}{n_2} = \cos u_1' - \cot i_1 \sin u_1'$$

$$= 1 - u_1' \cot i_1$$

to first degree in $|u_1'| < < \pi/2$. Therefore,

$$\frac{n_2 - n_1}{n_2} = \epsilon = u_1' \cot i_1 \tag{B2}$$

Since $|n_2 - n_1| < < 1$, $|u_1'| = |i_1 - i_1'| < < \pi/2$. For $y > 0$, that is, above the x-axis in figure 4, $u_1' > 0$ because $n_2 > n_1$ for a shock wave. Hence, the refraction is downward toward the optical axis.

Because of the point symmetry of the shock wave, the ray trace is symmetric about the line $\overline{OA}$ in figure 4. Therefore, $u_2' = 2u_1'$. Since, as originally defined (eq. (1)) $u \equiv u_2'$, this confirms the assumption $|u| < < \pi/2$ already made in the paraxial approximation.

Because $u_1' = u/2$, and considering figure 4,

$$\cot i_1 = \pm \left[\left(\frac{r}{y_1} \right)^2 - 1 \right]^{1/2} \tag{B3}$$

Therefore, equation (B2) finally becomes

$$\frac{n_2 - n_1}{n_2} = \frac{\delta}{2f'} \frac{r}{y_1} \left[1 - \left(\frac{y_1}{r} \right)^2 \right]^{1/2} \tag{6}$$

in terms of measurable quantities.

The distortion D is derived as follows:

$$\frac{D}{y_1} = \tan u_1' \tan u_2'$$

$$= \tan \left(\frac{u_2'}{2} \right) \tan u_2'$$

$$= \frac{u^2}{2} \tag{B4}$$

for small u. Hence, as a function of measurable quantities,

$$\frac{D}{y_1} = \frac{1}{2} \left(\frac{\delta}{f'} \right)^2 \approx 0 \tag{7}$$

An alternative form derivable from equations (B2) to (B4) and the condition $u = u_2' = 2u_1'$ is

$$\frac{D}{y_1} = 2\epsilon^2 \frac{(y_1/r)^2}{1 - (y_1/r)^2}$$

which displays the dependence on ϵ and the initial ray height y_1.

Axial ray-trace solution.—Ray-trace equations which are used to trace rays through a lens system in a step-by-step procedure can, in the present instance, be used to obtain simple, explicit approximations for ϵ and D without assuming $d = 2r$ and $r_1 = -r_2$.

Initially the incident ray height Q_1 (fig. 3) measured normal to the ray from the intersection of the optical axis with the first shock is given by (ref. 8, pp. 24 to 27)

$$Q_1 = s_1 \sin u_1$$

where s_1 is the axial distance from the shock to the intersection of the incident ray with the optical axis (fig. 3). At the first shock surface, Snell's law is

$$\sin i_1' = \frac{n_1}{n_2} \sin i_1$$

as before, where now

$$\sin i_1 = \frac{Q_1}{r_1} - \sin u_1$$

and

$$u_1' = u_1 + i_1 - i_1'$$

After refraction the ray height becomes

$$Q_1' = Q_1 \frac{\cos u_1' + \cos i_1'}{\cos u_1 + \cos i_1}$$

The ray is transferred to the second shock encounter by using the relations

$$Q_2 = Q_1' - d \sin u_1'$$

$$u_2 = u_1'$$

At the second surface,

$$\sin i_2' = \frac{n_2}{n_1} \sin i_2$$

where

$$\sin i_2 = \frac{Q_2}{r_2} - \sin u_2$$

and

$$u = u_2' = u_2 + i_2 - i_2'$$

Note from the preceding analyses that u is used to evaluate ϵ, so that Q_2' is not needed.

In the present problem the rays are initially parallel to the optical axis. Hence

$$u_1 = 0$$

$$Q_1 = y_1$$

so that

$$\sin i_1 = \frac{y_1}{r_1} \equiv a$$

$$\sin i_1' = \frac{n_1}{n_2} \frac{y_1}{r_1} \equiv a' = \frac{n_1}{n_2} a$$

$$u_1' = i_1 - i_1'$$

$$\equiv \sin^{-1} A$$

at the first surface, where (ref. 20)

$$A \equiv \pm \frac{y_1}{r_1} \left[1 - \left(\frac{n_1}{n_2} \frac{y_1}{r_1} \right)^2 \right]^{1/2}$$

$$\mp \frac{n_1}{n_2} \frac{y_1}{r_1} \left[1 - \left(\frac{y_1}{r_1} \right)^2 \right]^{1/2}$$

$$= \pm a \left(1 - a'^2 \right)^{1/2} \mp a' \left(1 - a^2 \right)^{1/2}$$

The upper signs apply if $n_2 > n_1$, and the lower signs apply if $n_2 < n_1$. Thus, the upper signs apply for shock waves, and the lower signs apply for expansion waves.

In terms of the new variables,

$$Q_1' = y_1 \frac{(1 - A^2)^{1/2} + (1 - a'^2)^{1/2}}{1 + (1 - a^2)^{1/2}}$$

and the transferred Q becomes

$$Q_2 = y_1 \frac{(1 - A^2)^{1/2} + (1 - a'^2)^{1/2}}{1 + (1 - a^2)^{1/2}} - dA$$

At the second surface,

$$u_2 = u_1' = \sin^{-1} A$$

$$i_2 = \sin^{-1} \left(\frac{Q_2}{r_2} - A \right)$$

$$i_2' = \sin^{-1} \left[\frac{n_2}{n_1} \left(\frac{Q_2}{r_2} - A \right) \right]$$

Therefore,

$$u = u_2' = \sin^{-1} A + \sin^{-1} \left(\frac{Q_2}{r_2} - A \right)$$

$$- \sin^{-1} \left[\frac{n_2}{n_1} \left(\frac{Q_2}{r_2} - A \right) \right]$$

In analogy with a, let

$$b \equiv \frac{Q_2}{r_2} - A$$

$$b' \equiv \frac{n_2}{n_1} \left(\frac{Q_2}{r_2} - A \right) = \frac{n_2}{n_1} b$$

and

$$B \equiv \mp b(1 - b'^2)^{1/2} \pm b'(1 - b^2)^{1/2}$$

where the upper and lower sign convention is the same as for A. Then,

$$u = \sin^{-1} A + \sin^{-1} B$$

For a gas lens,

$$\frac{n_1}{n_2} = 1 - \epsilon$$

$$\frac{n_2}{n_1} = \frac{1}{1-\epsilon} \approx 1 + \epsilon$$

to first degree in ϵ, so that

$$a' = (1-\epsilon)a$$

$$b' = (1+\epsilon)b$$

If

$$\frac{2\epsilon a^2}{1-a^2} < 1$$

then, as a function of a,

$$A = \pm \frac{\epsilon a}{(1-a^2)^{1/2}}$$

The inequality implies that

$$|a| = |y_1/r_1| < 0.999$$

for valid calculations. In other words, measurements of color should not be made too close to tangency to the shock wave. Analogously,

$$B = \mp \frac{\epsilon b}{(1-b^2)^{1/2}}$$

Paraxial rays: Assume $|y_1/r_1| < < 1$. Thus, $|a|$, $|a'|$, $|A|$, $|B| < < 1$, so that

$$Q_2 = y_1$$

$$b = -a$$

and

$$A = B = \pm \epsilon a$$

to first degree in ϵ. Therefore,

$$u = A + B = 2\epsilon a$$

so that, finally,

$$\frac{n_2 - n_1}{n_2} = \frac{\delta}{2f'} \frac{r}{y_1} \qquad (4)$$

which agrees with the thick gas lens equation (4), as it should.

Axial rays: For rays passing near, but not too near ($|y_1/r_1| < 0.999$), tangency to the shock wave, $|y_1/r_1|$ is less than unity. Then, $|a|$, $|a'|$, $|b|$, $|b'| < 1$, and $|A|$, $|B| < < 1$. As in the general approximation,

$$A = \pm \frac{\epsilon a}{(1-a^2)^{1/2}}$$

and

$$B = \mp \frac{\epsilon b}{(1-b^2)^{1/2}}$$

If $r_2 = -r_1$, and d is not very much greater than r_2, then to first degree in ϵ,

$$b = -a[1 - O(\epsilon)]$$

so that

$$u = A + B = \frac{2\epsilon a}{(1-a^2)^{1/2}}$$

Therefore,

$$\frac{n_2 - n_1}{n_2} = \frac{\delta}{2f'} \frac{r}{y_1} \left[1 - \left(\frac{y_1}{r}\right)^2 \right]^{1/2} \qquad (6)$$

for axial rays, in agreement with equation (6) obtained from Snell's law and symmetry considerations.

If the object plane includes the flow symmetry axis, or point, the distortion is given by

$$D = Y_o - y$$

where Y_o is the ordinate value of the intersection of the backward extension of the ray trace emergent from the lens with the object plane. Let Q_o and Q'_o represent perpendicular distances to a ray trace, respectively, within the lens and upon emergence from the lens measured from the center of the lens (fig. 4). Specifically,

$$Q_o = r_1 \sin i'_1 = r_2 \sin i_2$$

and

$$Q'_o = r_2 \sin i'_2 = (y_1 + D) \cos u$$

From the expression for Q_o and Snell's law, it follows that

$$\sin i_2' = -\sin i_1$$

Therefore,

$$D = y_1 \left(\frac{1}{\cos u} - 1 \right)$$

or

$$\frac{D}{y_1} = \frac{u^2}{2} \tag{B4}$$

for small u, as before.

Conical Lens

A given ray trace intercepts the cone

$$x^2 - 2rx + r^2 + y^2 - z^2 \tan^2 \theta \equiv g(x,y,z)$$

initially at $(x,y,z) = (x_1,y_1,z_1)$ and finally at $(x,y,z) = (x_2,y_2,z_2)$ (fig. 5(a)). The initial direction cosines of the ray are $(K,L,M) = (1,0,0)$. A normal to the cone is given by (ref. 21)

$$\hat{\mathbf{N}} = -\frac{\nabla g}{\sqrt{(\nabla g)^2}}$$

$$= -\frac{\hat{k}(x-r) + \hat{l}y - \hat{m}z \tan^2 \theta}{\left[(x-r)^2 + y^2 + z^2 \tan^4 \theta \right]^{1/2}}$$

where the caret denotes a unit vector. By virtue of the cone equation, the the equation for the unit normal reduces to

$$\hat{\mathbf{N}} = -\frac{\hat{k}(x-r) + \hat{l}y - \hat{m}z \tan^2 \theta}{z} \cot \theta \cos \theta$$

The direction cosines of the normal to the shock surface at the point (x_1,y_1,z_1) of initial incidence of the ray are

$$k_1 = -\frac{x_1 - r_1}{z_1} \cot \theta \cos \theta$$

$$l_1 = -\frac{y_1}{z_1} \cot \theta \cos \theta$$

$$m_1 = \sin \theta$$

However,

$$\cot \theta = \frac{z}{r}$$

where

$$r = (x^2 + y^2)^{1/2}$$

Therefore, when expressed as functions of quantities measurable in a y,z-plane, the direction cosines of the normal to the shock surface become

$$k_1 = \pm \left[1 - \left(\frac{y_1}{r_1} \right)^2 \right]^{1/2} \cos \theta$$

$$l_1 = -\frac{y_1}{r_1} \cos \theta$$

$$m_1 = \sin \theta$$

The cosine of the angle of incidence i of the ray at a surface is given by the scalar product of the direction cosines of the ray and the surface normal. At the first surface,

$$\cos i_1 = K_1 k_1 + L_1 l_1 + M_1 m_1 = k_1$$

$$= \pm \left[1 - \left(\frac{y_1}{r_1} \right)^2 \right]^{1/2} \cos \theta$$

The cosine of the angle of refraction i_1' is given, at the first surface, by

$$\cos i_1' = K_1' k_1' + L_1' l_1' + M_1' m_1'$$

$$= \left[1 - \left(\frac{n_1}{n_2} \right)^2 (1 - \cos^2 i_1) \right]^{1/2}$$

The direction cosines of the refracted ray are given by the components of the vector equation (ref. 8, p. 147),

$$n_2 \hat{\mathbf{R}}_1' = n_1 \hat{\mathbf{R}}_1 + (n_2 \cos i_1' - n_1 \cos i_1) \hat{\mathbf{N}}_1$$

where the carets denote unit vectors along the ray $\mathbf{R}$ and along the surface normal $\mathbf{N}$. Let

$$J_1 \equiv n_2 \cos i_1' - n_1 \cos i_1$$

so that

$$n_2\hat{\mathbf{R}}_1' = n_1\hat{\mathbf{R}}_1 + J_1\hat{\mathbf{N}}_1$$

Therefore, the direction cosines of the refracted ray are given by

$$K_1' = \frac{n_1}{n_2}K_1 + \frac{k_1}{n_2}J_1 = K_2$$

$$L_1' = \frac{n_1}{n_2}L_1 + \frac{l_1}{n_2}J_1 = L_2$$

$$M_1' = \frac{n_1}{n_2}M_1 + \frac{m_1}{n_2}J_1 = M_2$$

With regard to the rainbow schlieren, only

$$K_2' \equiv \cos u \approx 1 - \frac{1}{2}u^2$$

needs to be determined. In analogy with K_1',

$$K_2' = \frac{n_2}{n_1}K_2 + \frac{k_2}{n_1}J_2$$

$$= 1 + \frac{k_1}{n_1}J_1 + \frac{k_2}{n_1}J_2$$

where, in analogy with J_1,

$$J_2 \equiv n_1 \cos i_2' - n_2 \cos i_2$$

The next problem is to express the J's as functions of quantities more easily related to measurable quantities. Start with

$$J_1 = n_2 \cos i_1' - n_1 \cos i_1$$

In order to eliminate i_1', define

$$i_1 = \frac{\pi}{2} - \varphi_1 \qquad \varphi_1 < \frac{\pi}{2}$$

Then,

$$J_1 = n_2\left\{1 - \left(\frac{n_1}{n_2}\right)^2\left[1 - \cos^2\left(\frac{\pi}{2} - \varphi_1\right)\right]\right\}^{1/2}$$

$$- n_1 \cos\left(\frac{\pi}{2} - \varphi_1\right)$$

$$= n_2\left[1 - \left(\frac{n_1}{n_2}\right)^2 \cos^2 \varphi_1\right]^{1/2} - n_1 \sin \varphi_1$$

As in the circular case, let

$$\frac{n_1}{n_2} = 1 - \epsilon \qquad \epsilon << 1$$

so that

$$\left(\frac{n_1}{n_2}\right)^2 - 1 - 2\epsilon + \epsilon^2$$

and

$$J_1 = n_2\left[\sin^2 \varphi_1 + (2\epsilon - \epsilon^2) \cos^2 \varphi_1\right]^{1/2} - n_1 \sin \varphi_1$$

Assume

$$\sin^2 \varphi_1 = \cos^2 i_1 >> 2\epsilon$$

Then,

$$J_1 = n_2 \sin \varphi_1\left[1 + (2\epsilon - \epsilon^2) \cot^2 \varphi_1\right]^{1/2} - n_1 \sin \varphi_1$$

By expanding the square root, it follows that, to second degree in ϵ,

$$J_1 = \frac{n_2\epsilon}{\sin \varphi_1}\left(1 - \frac{1}{2}\epsilon \cot^2 \varphi_1\right)$$

so that

$$J_1 = \frac{n_2\epsilon}{\cos i_1}\left(1 - \frac{1}{2}\epsilon \tan^2 i_1\right)$$

By a similar argument i_2' can be eliminated from the expression for J_2. Thus, let

$$i_2 = -\frac{\pi}{2} + \varphi_2 \qquad \varphi_2 < \frac{\pi}{2}$$

so that

$$J_2 = n_1 \cos i_2'' - n_2 \cos i_2$$

becomes

$$J_2 = n_1 \left[1 - \left(\frac{n_2}{n_1}\right)^2 \cos^2 \varphi_2 \right]^{1/2} - n_2 \sin \varphi_2$$

Since $n_1/n_2 = 1 - \epsilon$,

$$\frac{n_2}{n_1} = \frac{1}{1-\epsilon} = 1 + \epsilon + \epsilon^2$$

and

$$\left(\frac{n_2}{n_1}\right)^2 = 1 + 2\epsilon + 3\epsilon^2$$

to second degree in ϵ. Therefore,

$$J_2 = n_1 \left[\sin^2 \varphi_2 - (2\epsilon + 3\epsilon^2) \cos^2 \varphi_2 \right]^{1/2} - n_2 \sin \varphi_2$$

In analogy with φ_1, assume that

$$\sin^2 \varphi_2 = \cos^2 i_2 >> 2\epsilon$$

so that

$$J_2 = -\frac{n_2 \epsilon}{\sin \varphi_2} \left(1 + \frac{1}{2} \epsilon \cot^2 \varphi_2 \right)$$

or

$$J_2 = -\frac{n_2 \epsilon}{\cos i_2} \left(1 + \frac{1}{2} \epsilon \tan^2 i_2 \right)$$

to second degree in ϵ.

When the preceding expressions for the J's are introduced in that for K_2', the result is

$$K_2' = 1 + \epsilon \left(1 - \frac{k_2}{\cos i_2} \right) + (\epsilon^2 + \epsilon^3)$$

$$\bullet \left(1 - \frac{k_2}{\cos i_2} - \frac{1}{2} \tan^2 i_1 - \frac{1}{2} \frac{k_2}{\cos i_2} \tan^2 i_2 \right)$$

where n_2/n_1 has been expanded to second degree in ϵ, and $k_1/\cos i_1 = 1$. Since the coefficients of the terms in ϵ^2 and ϵ^3 are identical, and $\epsilon \leq 0(10^{-3})$, the ϵ^3 term has negligible effect on K_2' in comparison with the ϵ^2 term.

The next step is to express $k_2/\cos i_2$ as a function of ϵ. Since

$$\cos i_2 = K_2 k_2 + L_2 l_2 + M_2 m_2$$

it follows that

$$\frac{\cos i_2}{k_2} = K_2 + L_2 \frac{l_2}{k_2} + M_2 \frac{m_2}{k_2}$$

$$= 1 - \epsilon(1 + a_1 a_2 \cot^2 \theta)$$

$$\bullet \left[(1 - a_1^2)(1 - a_2^2) \right]^{-1/2} \tan^2 \theta$$

to first degree in ϵ, so that

$$1 - \frac{k_2}{\cos i_2} \equiv -\epsilon h(a_1, a_2, \theta) << 1$$

where

$$h \equiv \frac{(1 + a_1 a_2 \cot^2 \theta) \tan^2 \theta}{\left[(1 - a_1^2)(1 - a_2^2) \right]^{1/2}}$$

$$a_1 \equiv y_1/r_1$$

$$a_2 \equiv y_2/r_2$$

Since $K_2' \approx 1 - (1/2)u^2$, the previous equation for K_2' reduces to

$$\epsilon = \frac{u}{\sqrt{2}} \left[h + \frac{1}{2} (\tan^2 i_1 + \tan^2 i_2) \right]^{-1/2}$$

where terms in ϵ^3 are negligible.

Next, i_1, and i_2 can be expressed as functions of a_1 and a_2, respectively, by recalling that

$$\cos i_1 = k_1 = \pm(1 - a_1^2)^{1/2} \cos\theta$$

and

$$\cos i_2 = k_2/(1 + \epsilon h)$$
$$= \pm \frac{(1 - a_2^2)^{1/2} \cos\theta}{1 + \epsilon h}$$

so that, after some simplification,

$$\tan^2 i_1 + \tan^2 i_2 = \frac{2 - a_1^2 - a_2^2}{(1 - a_1^2)(1 - a_2^2) \cos^2\theta} - 2$$
$$= \frac{\alpha_1 + \alpha_2}{\alpha_1 \alpha_2 \cos^2\theta} - 2$$

if $|\epsilon h| << 1$, and where

$$\alpha_1 \equiv 1 - a_1^2$$

$$\alpha_2 \equiv 1 - a_2^2$$

In terms of the new symbols

$$h + \frac{1}{2}\left(\tan^2 i_1 + \tan^2 i_2\right)$$
$$= \frac{(1 + a_1 a_2 \cot^2\theta) \tan^2\theta}{(\alpha_1 \alpha_2)^{1/2}} + \frac{\alpha_1 + \alpha_2}{\alpha_1 \alpha_2 \cos^2\theta} - 1$$
$$= \frac{1}{(\alpha_1 \alpha_2)^{1/2}} \left[\tan^2\theta + a_1 a_2 + \frac{\alpha_1 + \alpha_2 - 2\alpha_1 \alpha_2 \cos^2\theta}{2(\alpha_1 \alpha_2)^{1/2} \cos^2\theta}\right]$$

after some algebraic manipulations. When this is introduced in the preceding equations for ϵ, it becomes

$$\epsilon = \pm u \left\{\frac{\alpha_1 \alpha_2 \cos^2\theta}{[2(\alpha_1 \alpha_2)^{1/2} \sin^2\theta + 2a_1 a_2 (\alpha_1 \alpha_2)^{1/2} \cos^2\theta + \alpha_1 + \alpha_2 - 2\alpha_1 \alpha_2 \cos^2\theta]}\right\}^{1/2}$$

The final, lengthy, intermediate step is to express a_2 as a function of a_1. This involves transfer formulas which relate x_2, y_2, z_2 to x_1, y_1, z_1. The transfer formulas for the cone are (figs. 5(b) and (c))

$$x_2 = K_1'\Delta + x_1 - \frac{1}{2}(d_1 + d_2)$$

$$y_2 = L_1'\Delta + y_1$$

$$z_2 = M_1'\Delta + z_1$$

where Δ is the path length of the ray trace within the lens, and $d = 2r$ is the diameter of the circular cross section of the cone. Specifically, $d_1 = 2r_1$ and $d_2 = -2r_2$. Introduce the ray-trace coordinates at the second shock surface into the original cone equation, so that

$$\left(x_2 - \frac{1}{2}d_2\right)^2 + y_2^2 - z_2^2 \tan^2\theta = 0$$

where

$$X = x_2 - \frac{1}{2}d_2$$

$$Y = y_2$$

$$Z = z_2$$

Substituting the right-hand sides of the transfer formulas into the new cone equation results in the quadratic equation

$$\left[K_1'\Delta + x_1 - \frac{1}{2}(d_1 + d_2)\right]^2 + (L_1'\Delta + y_1)^2$$
$$- (M_1'\Delta + z_1)^2 \tan^2\theta = 0$$

This equation possesses the solution

$$\Delta = -\mathcal{F} \pm (\mathcal{F}^2 - \mathcal{G})^{1/2}$$

where

$$\mathcal{F} \equiv \frac{K_1'\left[x_1 - \frac{1}{2}(d_1 + d_2)\right] + L_1' y_1 - M_1' z_1 \tan^2\theta}{K_1'^2 + L_1'^2 - M_1'^2 \tan^2\theta}$$

and

$$\mathcal{G} \equiv \frac{\left[x_1 - \frac{1}{2}(d_1 + d_2)\right]^2 + y_1^2 - z_1^2 \tan^2 \theta}{K_1'^2 + L_1'^2 - M_1'^2 \tan^2 \theta}$$

In order to evaluate $a_2 \equiv y_2/r_2$, note that

$$y_2 - y_1 = L_2 \Delta$$

from the transfer formula. To first degree in ϵ,

$$L_2 = -\epsilon a_1 (1 - a_1^2)^{-1/2}$$

Since $L_2 = O(\epsilon)$, terms involving ϵ can be neglected in the contribution of Δ to $y_2 - y_1$. Therefore,

$$\Delta = \frac{1}{2}(d_1 + d_2) - x_1$$

But,

$$x_1 = r_1 \left[1 - (1 - a_1^2)^{1/2}\right]$$

and from figure 5(a),

$$d_2 = 2z_2 \tan \theta$$

so that

$$\Delta = \frac{1}{2}d_1 + z_2 \tan \theta - r_1\left[1 - (1 - a_1^2)^{1/2}\right]$$

By virtue of the transfer formula,

$$z_2 = z_1 + M_1' \Delta$$

it follows that

$$z_2 = z_1[1 + O(\epsilon)]$$

so that

$$\Delta = r_1\left[1 + (1 - a_1^2)^{1/2}\right]$$

Since

$$y_2 = y_1[1 - O(\epsilon)]$$

and

$$r_2 = z_2 \tan \theta$$
$$= z_1 \tan \theta[1 + O(\epsilon)]$$
$$= r_1[1 + O(\epsilon)]$$
$$a_2 = a_1[1 - O(\epsilon)] \approx a_1$$

Therefore,

$$\alpha_1 \approx \alpha_2 \equiv \alpha$$

With these approximations the preceding equation for ϵ becomes

$$\epsilon = \pm \frac{u}{\sqrt{2}} \left[\frac{\alpha^2 \cos^2 \theta}{(\alpha \sin^2 \theta + a_1 \alpha \cos^2 \theta + \alpha - \alpha^2 \cos^2 \theta)}\right]^{1/2}$$

which reduces to

$$\epsilon = \pm \frac{u}{2}\left[\frac{1 - (y_1/r)^2}{1 + (y_1/r)^2 \cot^2 \theta}\right]^{1/2} \cot \theta$$

or in terms of quantities measurable with a rainbow schlieren,

$$\epsilon = \pm \frac{\delta \cot \theta}{2f'}\left[\frac{1 - (y_1/r)^2}{1 + (y_1/r)^2 \cot^2 \theta}\right]^{1/2} \tag{8}$$

Appendix C

Interference Fringe − Shift Equation for Spherical or Cylindrical Gas Lens

The fringe shift S at wavelength λ is given by

$$S\lambda = \psi_1 - \psi_2$$

where ψ is the optical path length along a ray trace. The difference made evident by symmetry considerations is (fig. 6)

$$\psi_1 - \psi_2 = 2n_2 r \cos i_1' - 2n_1(r \cos i_1 + y_1 \tan u_1')$$

where the first term refers to the ray trace through the lens, and the other term refers to the reference ray trace through the ambient medium. Expressing quantities in alternative forms defined in appendix B gives the quadratic equation

$$\frac{a^2}{1-a^2}\epsilon^2 + \epsilon - \frac{S\lambda}{2r(1-a^2)^{1/2}} = 0$$

Its solution is

$$\epsilon = \frac{S\lambda}{2r(1-a^2)^{1/2}}$$

from which it follows that

$$\frac{S}{2r(1-a^2)^{1/2}} = \frac{\epsilon}{\lambda} = \text{constant}$$

References

1. Marcuse, Dietrich: Light Transmission Optics. Second Ed., Van Nostrand Reinhold Co., 1982, pp. 144-163.
2. Howes, W.L.: Rainbow Schlieren. NASA TP-2166, 1983.
3. Howes, W.L.: Rainbow Schlieren and Its Applications. Appl. Opt., vol. 23, no. 14, July 15, 1984, pp. 2449-2460
4. Whitham, G.B.: Linear and Nonlinear Waves. John Wiley & Sons, 1974.
5. Weinberg, F.J.: Optics of Flames. Butterworths, Washington, D.C., 1963, pp. 24-26.
6. Equations, Tables, and Charts for Compressible Flow. NACA Rept. 1135, 1953.
7. Hardy, A.C.; and Perrin, F.H.: The Principles of Optics. McGraw-Hill, 1932.
8. Kingslake, R.: Lens Design Fundamentals. Academic Press, 1978.
9. Weimer, D.: Pockels-Effect Cell for Gas-Flow Simulation. NASA TP-2007, 1982.
10. Mihora, D.J.: Data Appendix: F−Number = 1.0 EMR With a Flexible Back Electrode. (CR-4-998, General Research Corp.; NASA Contract NAS1-16133) NASA CR-172477, 1984.
11. Kendall, J.M., Jr.: Acoustic Lens is Gas Filled. NASA Tech. Briefs, vol. 5, no. 3, Fall 1980, pp. 345-346.
12. Foil Mirrors Make a Nice Reflection. Lasers and Applications, vol. 3, Nov. 1984, pp. 22, 24.
13. Frost, K.J.; and McDonald, F.B.: Space Research in the Era of the Space Station. Science, vol. 226, no. 4681, Dec. 21, 1984, pp. 1381-1385.
14. Kozichaiow, Eugene: SDI Revives Navy Laser Effort. Aviat. Week Space Technol., vol. 122, no. 8, Feb. 25, 1985, p. 26.
15. Bernatowicz, Daniel J.: Lewis Tackles Engineering Challenges for Complex Space Station Power Package. NASA Lewis Research Center = Lewis News, vol. 22, no. 3, Feb. 8, 1985, pp. 2-3.
16. Yonas, G.: Strategic Defense Initiative: The Politics and Science of Weapons in Space. Phys. Today, vol. 38, no. 6, June 1985, pp. 24-32.
17. Goslee, J.W.; Hinson, W.F.; and Davis, W.T.: Electrostatic Forming and Testing of Polymer Films on a 16-Foot Diameter Test Fixture. NASA TM-86328, 1985.
18. Lucas, J.W.: Parabolic Dish Solar Thermal Power Annual Program Review, Proceedings. (JPL-PUB-82-66, Jet Propulsion Lab; NASA Contract NAS7-100) NASA CR-169365, 1982.
19. Smith, W.J.: Modern Optical Engineering. McGraw-Hill, 1966, pp. 385-398.
20. Abramowitz, M.; and Stegun, I.A., Eds.: Handbook of Mathematical Functions. Dover Publications, 1965, p. 80, formula 4.4.32.
21. Hildebrand, F.B.: Advanced Calculus for Engineers. Prentice-Hall, 1949, p. 309.

1. Report No. NASA TP-2555	2. Government Accession No.	3. Recipient's Catalog No.
4. Title and Subtitle Optical Elements Formed by Compressed Gases – Analysis and Potential Applications		5. Report Date January 1986
		6. Performing Organization Code 505-40-14
7. Author(s) Walton L. Howes		8. Performing Organization Report No. E-2561
		10. Work Unit No.
9. Performing Organization Name and Address National Aeronautics and Space Administration Lewis Research Center Cleveland, Ohio 44135		11. Contract or Grant No.
		13. Type of Report and Period Covered Technical Paper
12. Sponsoring Agency Name and Address National Aeronautics and Space Administration Washington, D.C. 20546		14. Sponsoring Agency Code

15. Supplementary Notes

16. Abstract

Spherical, cylindrical, and conical shock waves are optically analogous to gas lenses. The geometrical optics of these shock configurations are analyzed as they pertain to flow visualization instruments, particularly the rainbow schlieren apparatus and single-pass interferometers. It is proposed that a lens or mirror formed by gas compressed between plastic sheets has potential as a fluid visualization test object; as the objective mirror in a very large space-based telescope, communication antenna, or energy collector; as the objective mirror in inexpensive commercial telescopes; and as a component in fluid visualization apparatuses.

17. Key Words (Suggested by Author(s)) Gas lens, Gas-supported mirror, Rainbow schlieren, Telescope, Antenna	18. Distribution Statement Unclassified – unlimited STAR Category 74		
19. Security Classif. (of this report) Unclassified	20. Security Classif. (of this page) Unclassified	21. No. of pages 22	22. Price A02

National Aeronautics and
Space Administration
Code NIT-4

Washington, D.C.
20546-0001

NASA

POSTMASTER: If Undeliverable (Section 158
Postal Manual) Do Not Return